

Light-induced atomic desorption and diffusion of Rb from porous alumina

S. Villalba, H. Failache and A. Lezama

*Instituto de Física, Facultad de Ingeniería, Universidad de la República,
J. Herrera y Reissig 565, 11300 Montevideo, Uruguay*

(Dated: February 13, 2022)

We present the first study of light induced atom desorption (LIAD) of an alkali atom (Rb) in porous alumina. We observe the variation due to LIAD of the rubidium density in a vapor cell as a function of illumination time, intensity and wavelength. The simple and regular structure of the alumina pores allows a description of the atomic diffusion in the porous medium in which the diffusion constant only depends on the known pore geometry and the atomic sticking time to the pore wall. A simple one-dimensional theoretical model is presented which reproduces the essential features of the observed signals. Fitting of the model to the experimental data gives access to the diffusion constant and consequently the atom-wall sticking time and its dependence on light intensity and wavelength. The non-monotonic dependence of the LIAD yield on the illumination light frequency is indicative of the existence of Rb clusters in the porous medium.

PACS numbers: 68.43.Tj 66.30.Pa 78.67.Rb 47.61.-k 78.67.Bf

I. INTRODUCTION

In a spectroscopic cell containing an alkali atom vapor, a substantial fraction of the atoms are adsorbed on the cell walls. At steady state, the gas density is in equilibrium with the adsorbed atomic fraction. In some cells, depending on the cell material or coating, when the cell is illuminated with moderate intensity (1 - 1000 mW/cm²) nonresonant light, a significant increase in the atomic vapor density is produced as a consequence of the release of atoms from the cell surface into the gas phase. Such effect has been named light induced atomic desorption (LIAD) [1].

LIAD has received considerable attention in recent years due to its application as a light-controlled atom dispenser under high vacuum conditions. Such dispenser has been successfully used to load magneto-optical atom traps [2, 3, 4] and hollow optical fibers [5, 6, 7]. Its use has also been considered for atomic magnetometers, gyroscopes and clocks [8, 9]. In addition, LIAD has attracted the attention of astrophysicists since it has been related to the observed abundance of alkaline elements in nonpermanent extraterrestrial atmospheres [10].

LIAD is understood as a non-thermal effect as opposed to light desorption produced with high power sources in which a significant heating results from light absorption by the substrate. In poly-dimethylsiloxane (PDMS) [11], paraffin [12] and sapphire [13] a frequency threshold in the infrared, similar to that of the photoelectric effect on metals, has been observed. Also, an increasing efficiency of LIAD with light frequency has been reported in several samples [12, 14, 15].

LIAD was first observed in sodium vapor glass cells in which the inner cell walls were coated with a thin layer of PDMS. The effect was also observed with K [16], Rb and Cs atoms [12] (sometimes in the presence of a buffer gas). Initially, it was considered that LIAD was specific to PDMS coatings [11]. However, LIAD was

later-on reported in cells coated with different polymers such as octadimethyl-cyclotetrasiloxane (OCT) [17] and paraffin [12]. LIAD has also been observed on several uncoated surfaces such as glass [4, 7], stainless steel [4] and sapphire [18]. More recently, LIAD has been studied in porous amorphous materials such as porous silica [19]. All observations of LIAD in porous or coated surfaces present some common features such as the characteristic time scale of the atomic desorption (several seconds). However, other aspects may vary significantly between different atomic species and coatings depending also in the cell preparation procedure. In particular, large variations are observed in the desorption yield. In cells coated with PDMS, LIAD may result in an increase of the atomic gas phase density of several orders of magnitude [11] while only density-increase-factors of a few units were reported for paraffin [12]. Smaller factors were observed on uncoated surfaces as in the present study. The question on whether there is a common mechanism underlying all LIAD observations is still open [20].

The first tentative explanation of LIAD at the microscopic level was suggested by Xu et al [11]. The mechanism involves the modification by light of the weakly bonded chemical complex formed between a PDMS molecule and the Na atom or Na₂ molecule. More recently, this mechanism was further investigated through the measurement of the thermal distribution of desorbed atom velocities [21]. This interpretation of LIAD is consistent with the observation of a threshold light frequency for LIAD in PDMS but leaves unexplained several aspects of its dynamics. As discussed by Atutov et al [14], in addition to the atomic desorption from the surface, the diffusion of the atoms within the surface coating plays an essential role in the temporal evolution of LIAD. To a large extent, LIAD in coated surfaces is a consequence of light-induced modification of the atomic mobility and diffusion within the coating polymer. Atutov et al [14] have modelled such process

assuming a phenomenological dependence of the diffusion coefficient on light. Alexandrov et al have described the LIAD dynamics with the help of rate equations with a light dependent term representing the flux of atoms from the coating into the gas phase [12]. Recently, the model of LIAD in coated surfaces suggested by Atutov has been revised and improved by Rebilas and co-workers [22, 23].

LIAD from uncoated dielectric surfaces, such as sapphire or glass, deserves special consideration. In such systems, alkaline atoms can be individually adsorbed on the surface or agglomerated into clusters. The presence of clusters may result in a visible change of the sample transparency or even in coloration [24]. Blue-green coloration by Rb of otherwise transparent (or white) samples has been observed in several experiments including the ones described here. The role of the light in these samples is double since it can produce the direct desorption of the atoms from the dielectric surface and the evaporation of the atomic clusters [25, 26]. Also, under suitable conditions, the light may also control the growth of the clusters from atoms in the vapor phase. Such conditions are favored in porous media where the desorbed atoms remain confined and available to participate in the cluster regrowth. A characteristic feature of the LIAD involving cluster evaporation, is the non-monotonic dependence of the desorption yield on the light frequency. Such behavior is interpreted as the consequence of resonant surface plasmon excitation in the cluster [25]. A second characteristic of these systems is its “memory”. The response strongly depends on the illumination history including the timing of the bright and dark periods and the corresponding color sequence [25].

A common feature governing the dynamics of both, the LIAD in polymer coated surfaces and in porous dielectrics, is the successive occurrence of two distinctive processes: i) atomic desorption from the surface (or cluster) ii) diffusion in the intermediate medium (either the polymer or the porous medium) prior to the atom release in the vapor phase. A precise modelling of LIAD should involve the simultaneous account of these two processes. The desorption mechanism is at present only qualitatively understood [11, 21, 25]. Also, little understanding is currently available on the mechanisms determining the variation with light of the atomic mobility in the polymer coating. Diffusion in porous silica is presumably simpler since the atomic motion inside the pores may be assumed to occur in a diluted vapor. However, the random nature of the pore geometry complicates the modelling of such process.

In this paper we present the experimental study and theoretical modelling of LIAD with Rb atoms adsorbed in thin membranes of porous alumina. The porous medium is produced by anodization of aluminum and results in a very regular array of cylindrical pores with small size dispersion. The average diameter of the pore tube is 200 nm and its length 60 μm . In consequence,

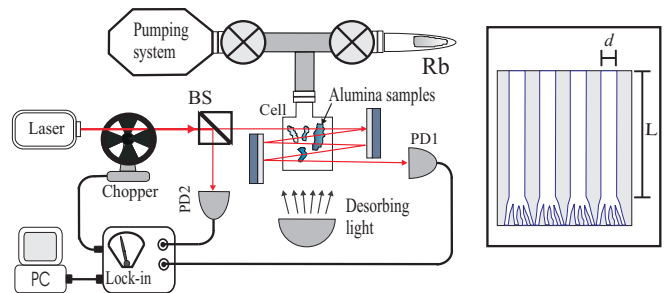


FIG. 1: (Color online) Experimental setup. Inset: Schematic cut of the alumina membrane for a plane parallel to the pores. BS: beam splitter, PD1, PD2: photodetectors.

the pore geometry is well known and this allows a simple and accurate description of the atomic diffusive motion in the pore. The diffusion process is the result of a random sequence of atomic free flight of the atoms confined within the pore wall. After a collision with the wall, the atom sticks to the wall for some time after which it is desorbed again flying with random direction and velocity. Under such assumptions, the diffusive part (ii) of the LIAD dynamics, including the release of atoms into the gas phase, is determined by the pore geometry and the atom-surface sticking time. Such picture allows us to model the atomic diffusion in the pores as well as the atom exchange between the porous material and the outside gas volume. The resulting LIAD dynamics is mainly dependent on the atomic diffusion constant in the porous medium which can be obtained from the fitting of the observed variation of the atomic density in the gas phase. From the knowledge of the diffusion constant, the atom-wall sticking time can be determined. We have investigated the variation of the sticking time with light intensity and color.

II. EXPERIMENT

We have used porous alumina membranes manufactured by Whatman International Limited. The circular flat membranes have a diameter of one inch and a thickness of 60 μm . The membrane is traversed by a regular array of cylindrical hollow tubes with 200 nm diameter. The tubes form a honey comb like array with a pore density of $10^9/\text{cm}^2$. The diameter of the pores are uniform over most of their length. On one side of the membrane, along 1 μm , the pores divide into several smaller branches with 20 nm typical diameter (see the inset in Fig. 1). Before contact with the Rb vapor the porous membranes are translucent and white. In order to fit into the vacuum glass cell, the membranes are divided in pieces of typically 0.5 cm^2 .

The experimental setup is shown in Fig. 1. We have used a vacuum glass cell with 2.5 x 2.5 x 4.5 cm dimensions. The cell is connected via a glass-to-metal tran-

sition fitting to an ion pump and a metallic Rb reservoir. The Rb density in the glass cell is monitored by measuring the absorption of a laser beam issued from an extended cavity diode laser. Using a saturated absorption setup, the laser frequency is stabilized to the ^{85}Rb $F = 3 \mapsto F' = 4$ transition in the D2 line (780 nm). In order to increase the absorption signal, the laser beam crosses the cell several times. We have used a balanced detection scheme to reduce sensitivity to laser intensity fluctuations. Half of the laser power is sampled before the cell and detected with a photodiode. A second photodiode monitors the intensity of the beam transmitted through the cell. The outputs of the two photodiodes are subtracted. In order to eliminate noise from ambient light, including the light used for the LIAD, the laser beam is modulated with a chopper and lock-in detected. The illumination of the porous alumina samples is made with high power LEDs (100 mW) in order to have a non-thermal source with a well defined spectrum. Three different LEDs were used centered at 455, 504 and 617 nm (typical spectral width 10 nm). An optical arrangement (not shown in Fig. 1) allows a uniform illumination of the porous sample by the LED light.

Prior to the introduction of the porous alumina membrane, the glass cell was evacuated (10^{-6} torr) and baked for several hours at 300 C. Such precaution appeared to be essential since we have observed significant LIAD from the unbaked cell presumably due to some uncontrolled coating. After the baking procedure, the LIAD from the cell walls was negligible. Following the cell cleanup, several pieces of the alumina membrane were introduced and vacuum baked for several days at 150 Celsius. The pieces of alumina lied on the cell bottom. We had no control on the side of the membrane that faces the cell wall, so some of the pieces present the largest pore apertures toward the cell bulk volume while others present the narrow ramification ends. After the initial cleanup of the alumina, the cell was returned to room temperature and the valve separating the cell from the metallic Rb reservoir opened. Keeping the Rb reservoir and the vacuum connecting tubes slightly heated (~ 50 C), the Rb was allowed to diffuse into the cell and the porous alumina. After a few days, a visible blue coloration appeared in the alumina indicating the presence of Rb. After a sufficiently long period all the samples were dark blue. However two different blue tones were observed among the samples. We interpret such difference as a consequence of the two possible orientations of the membrane pieces with respect to the cell wall. The blue coloration is an indication of the formation of Rb clusters [24]. We have checked that the cluster formation is entirely reversible. The original white coloration of the alumina could be recovered after pumping the cell during a few hours while illuminating with an incandescent lamp.

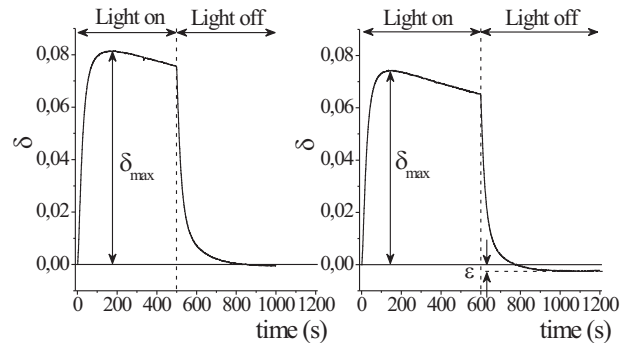


FIG. 2: Typical observed variations of the relative atomic vapor density for two different illumination-time intervals.

III. EXPERIMENTAL RESULTS

We have observed the LIAD of Rb from the porous alumina by monitoring the laser absorption in the cell bulk while turning on and off the illumination by a LED. We have recorded the relative variation of the vapor density $\delta(t) \equiv (\rho(t) - \rho_0)/\rho_0$ as a function of time where $\rho(t)$ is the density of Rb in the cell and ρ_0 the equilibrium density in the dark. Fig. 2 shows two typical records obtained with the same illumination for two different light-on intervals (500 and 600 s). In general, the relative density reaches a maximum δ_{max} after a few tens of seconds depending on light intensity. After that the Rb density slowly decreases towards a new steady state in the presence of light. When the light is turned off, δ decreases on a time scale comparable to the rise time. Two different behaviors have been observed for long times after the light switching off. Either the density returns monotonically to the initial equilibrium density ρ_0 or drops below ρ_0 by an amount ϵ (see Fig. 2) after what it slowly grows towards ρ_0 . The later behavior is observed if the light intensity and the illumination interval are sufficiently large.

Fig. 3 shows the evolution of the Rb density in the cell for two different illumination intensities. Notice the variation in the shape of the trace. Similar shape variations were also observed in experiments with porous silica [19], although not reproduced by the proposed theoretical models.

We have observed that the efficiency of the LIAD process depends on the porous alumina history, as was also noticed in other systems [12, 25]. A monotonic reduction in the maximum relative Rb density variation δ_{max} is observed for several successive illumination cycles keeping constant the light intensity. In addition, as the intensity is changed between successive illumination periods, the signal variation is different depending on whether the light intensity is increased or decreased (see Fig. 4). For low enough light intensities the system is not appreciably

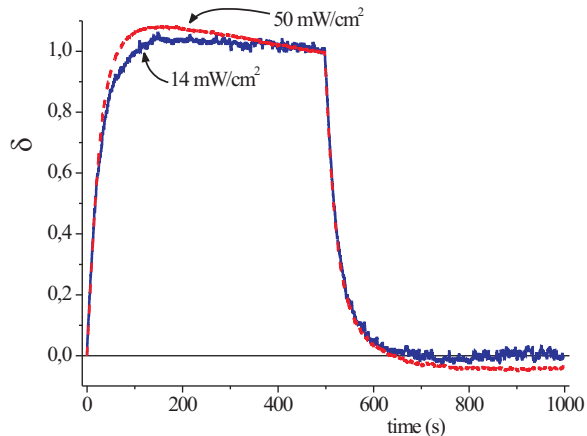


FIG. 3: (Color online) Two records of the relative atomic density variation illustrating the difference in shape for different illumination intensities. The traces have been re-scaled to signal the difference in shape.

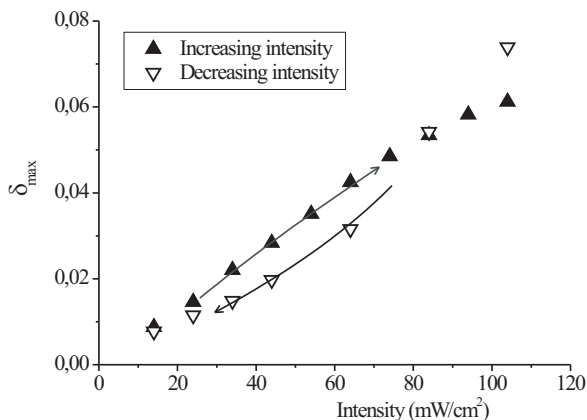


FIG. 4: Maximum relative atomic density δ_{max} as a function of the illumination intensity. The measurements were registered with a sequence of illumination intervals of 140s followed by intervals of 600s without illumination. Solid(hollow) triangles: increasing(decreasing) illumination intensity.

modified by the illumination and a linear dependence of the LIAD yield on light intensity is observed. The non-linear dependence, visible in Fig.4 for large intensities, can be attributed to the depletion of the available Rb inside the nano-pores.

Fig. 5 shows δ_{max} as a function of illumination intensity for three different wavelengths. The measurements were taken alternating the three available light colors successively for each intensity. The effect of the history on the LIAD efficiency is so reduced for the comparison among measurements taken with different

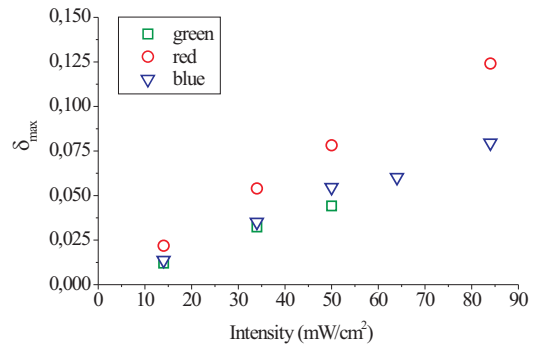


FIG. 5: (Color online) Maximum relative atomic density δ_{max} as a function of the illumination intensity for different illumination wavelengths (455, 505 and 617 nm).

wavelengths. In Fig.5 the non-linear variation of δ_{max} is only noticeable for the highest intensities.

From the linear fit of the data in Fig. 5 one can evaluate, for each wavelength, the coefficient $\alpha_\lambda \equiv \delta_{max} \hbar \omega / I$ proportional to the LIAD desorption rate per photon flux. We observe that this coefficient for blue, green and red light varies in proportion to 1, 0.73 and 1.1 respectively. Such result indicate a non-monotonic evolution of the LIAD yield with photon energy.

IV. THEORETICAL MODEL

We model the evolution of the atomic density inside the cylindrical pores as a one-dimensional diffusion process. The typical sticking time τ_s of alkali atoms on dielectric surfaces is of the order of tens to hundreds microseconds. After desorption, the atoms leave the internal surface of the pore with thermal velocity in a random direction with a Lambertian probability distribution [27]. The gas density inside the pores is considered sufficiently low to neglect the collisions between flying atoms. At room temperature and for hundred nanometers tube diameters, after a few nanoseconds flight, the atom is again adsorbed on the pore surface. Since the pore length is much larger than its diameter, we can consider that the atoms execute a one dimensional random walk, along the pore axis, characterized by the diffusion constant (see Appendix):

$$D = \frac{l^2}{2\tau} = \frac{d^2}{3\tau} \quad (1)$$

Where l^2 is the mean square displacement per step in the random walk, τ is the mean interval between steps which is essentially determined by the sticking time $\tau \simeq \tau_s$ on the internal pore surface and d is the pore diameter.

The atomic desorption is described by a reduction of τ_s induced by the light. We assume a simple linear de-

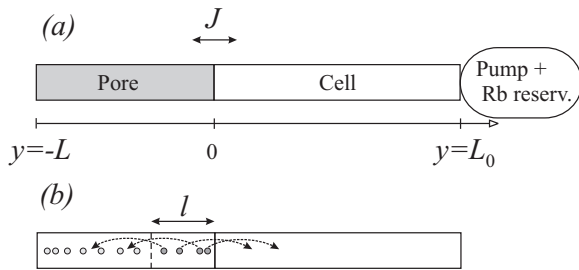


FIG. 6: a) Schematic one-dimensional model for the system. b) Illustration of the atomic release from the pore end into the gas cell (J^+ in Eq. 8).

pendence:

$$\tau_s = \tau_{s0}(1 - \kappa I) \quad (2)$$

where τ_{s0} is the sticking time in the dark, I is the light intensity and κ a coefficient which is wavelength dependent. In consequence:

$$D = \frac{D_0}{(1 - \kappa I)} \quad (3)$$

with $D_0 = d^2/(3\tau_{s0})$ being the atomic diffusion constant in the dark.

Fig. 6 present a scheme of the one-dimensional model of the system. The cylindrical pore, considered closed on its left end has a total length L . To the right of the pore, the atomic vapor cell, associated to a length L_0 , is connected to a reservoir accounting for the vacuum pumping and the external Rb reservoir.

The (linear) density of atoms $\mu(y, t)$ inside the pore is described by the diffusion equation

$$\frac{\partial \mu}{\partial t} = D \frac{\partial^2 \mu}{\partial y^2} \quad (4)$$

where y is the position coordinate inside the pore (see Fig.6).

The total number of atoms N in the cell is $N = N_g + N_w$ where N_g represents the atoms in the gas phase and N_w the atoms adsorbed to the cell wall. The fraction of atoms in the gas phase relative to the total number of atoms is assumed to be a constant for given temperature and illumination conditions [28]:

$$\frac{N_g}{N} = \frac{L_0}{L_0 + \Delta} \quad (5)$$

Here Δ represents an effective cell length corresponding to adsorbed atoms. Since the sticking time of the atoms to the cell walls can depend on light intensity, we consider that Δ depends on the illumination in the form: $\Delta = \Delta_0(1 - \zeta I)$ where ζ is a coefficient that can depend on

wavelength. The evolution of the atom number N in the cell is described by the equation

$$\frac{dN}{dt} = \frac{dN_g}{dt} \left\{ 1 + \frac{\Delta}{L_0} \right\} = J - \gamma(N_g - N_{g0}) \quad (6)$$

where J is the net atomic flux at the pore-vapor interface. The rate γ describes the return to the equilibrium atom number N_{g0} determined by the external pumping system and Rb reservoir.

We separate the net flux J into two contributions $J = J^+ + J^-$ describing the atoms leaving and entering the pore respectively. The flux of atoms entering the pores from the cell gas is given by:

$$J^- = -\frac{\bar{v}}{2L_0}N_g, \quad (7)$$

where $\bar{v} \equiv \langle |v_y| \rangle$ is the mean magnitude of the atomic velocity in the direction of the pore. The simple geometry of our system allows the evaluation of J^+ without additional assumptions by considering that the atoms within a mean step length l from the pore end have a probability 1/2 for leaving the pore in the time interval τ (see Fig. 6 b), then

$$J^+ = [\mu(0)l] \frac{1}{2\tau} \simeq \mu(0) \frac{D}{l}. \quad (8)$$

The equations describing the evolution of the atomic densities μ and $n \equiv N_g/L_0$ inside the pores and in the cell gas phase respectively are:

$$\frac{\partial \mu}{\partial t} = D \frac{\partial^2 \mu}{\partial y^2} \quad (9a)$$

$$\frac{dn}{dt} = \frac{D}{lL_c(1 - \sigma I)} \mu(0) - \frac{\left(\tilde{\gamma} + \frac{\bar{v}}{L_c}\right)}{(1 - \sigma I)} n + \frac{\tilde{\gamma}}{(1 - \sigma I)} n_0 \quad (9b)$$

where we have introduced the parameters $\sigma \equiv \frac{\zeta}{(1 + \frac{L_0}{2\Delta_0})}$,

$L_c \equiv (L_0 + \Delta)$ and $\tilde{\gamma} \equiv \frac{\gamma_0 L_0}{L_c}$. n_0 is the equilibrium value of the atomic density in the vapor cell.

The steady state densities in the dark inside the pores μ_0 and in the vapor cell n_0 are linked through the condition:

$$J = \frac{D_0}{l} \mu_0 - \frac{\bar{v}}{2} n_0 = 0. \quad (10)$$

The boundary conditions at the pore ends are (see Eqs. 7 and 8):

$$-D \frac{\partial \mu}{\partial y} \Big|_{y=0} = \frac{D}{l} \mu(0) - \frac{\bar{v}}{2} n \quad (11a)$$

$$\frac{\partial \mu}{\partial y} \Big|_{y=-L} = 0 \quad (11b)$$

From the above equations, it is possible to derive an approximate relation between the observed variation of the gas density in the cell and the corresponding change in the diffusion constant inside the pores. For this we notice that in our system, the return to equilibrium (under constant illumination) occurs on time scale which is long compared to the observation time. One can then consider that during the LIAD the total atomic population (inside the pores and in the cell) remains approximately constant:

$$\mu L + nL_c \simeq \left(\frac{l\bar{v}}{2D_0} L + L_c \right) n_0 \quad (12)$$

where we used Eq. 10.

When the sample is illuminated, the LIAD effect redistribute the atoms along the pore in a characteristic diffusion time $L^2/2D$. If we assume that the gas phase density reaches its maximum n_{max} in a time which is long compared to the diffusion time, one can consider that the corresponding atomic density inside the pores is approximately uniform $\mu \simeq \mu_{max}$. Using Eqs. 6 (with $\gamma = 0$) and 12 we have:

$$\delta_{max} \approx \frac{n_{max} - n_0}{n_0} = \frac{\Delta D}{D_0} \frac{1}{\left(1 + \frac{2DL_c}{\bar{v}lL}\right)} \quad (13)$$

Eq. 13 can be used for a quick estimate of the relative variation of the diffusion constant from the observed change in the vapor density, provided the second term inside the brackets in Eq. 13 is small. In the conditions of our experiment such term is of the order of unity.

Some of the parameters appearing in the model can be directly determined for our system. From the porous alumina manufacturer we know that $L = 60\mu m$, and $d = 200nm$. In consequence, $\langle l^2 \rangle = \frac{2}{3}d^2 \approx 1.6 \times 10^{-7}m^2$. The mean atomic velocity at room temperature is $\bar{v} \approx 140m/s$. The other parameters are determined through least square fitting of the numerical model to the experimental data. For this, we have numerically integrated the differential equations 9 with the boundary conditions given in Eqs. 11.

Fig. 7 shows a typical experimental register together with the corresponding signal calculated from the model. The values of the parameters obtained from the fitting are presented in Table. I. The given uncertainties correspond to the scattering of the results of the fitting for different experimental runs. The value of D_0 given in Table I results from the average of the data obtained with all three excitation wavelength. Interestingly enough, the plot of the fitted values of D_0 for different runs reveal a systematic grouping for each of the three colors used for LIAD (see Fig. 8). In our model, D_0 corresponding to the diffusion constant in the dark, is taken as constant and independent of the desorbing light color. However, the grouping observed in Fig. 8 may reveal a dependence of D_0 on the illumination history. Such feature could be

an indication of cluster formation and cluster-light interaction. The investigation of cluster formation is outside the scope of this work.

We notice that the value of L_0 in Table I is large compared to the length ($\lesssim 10m$) estimated from the actual glass cell volume. However, the total effective volume available to the atoms outside the porous alumina also depends on the vacuum system tubes and surfaces [8]. The parameter σ reflects the dependence of the effective cell length on the illumination. The numerical fitting is quite insensitive to this parameter giving a large scattering of the results. The uncertainty in this parameter prevents the determination of a wavelength dependence. On the other hand, different values of the coefficient κ are obtained depending on the wavelength of the illuminating light.

From the parameters in Table I we can check that the assumptions made for the derivation of Eq. 13 are reasonable for our system. The estimate of the maximum relative vapor density variation obtained using Eq. 13 only differs in a few percents from the value resulting from the numerical integration of Eqs. 9.

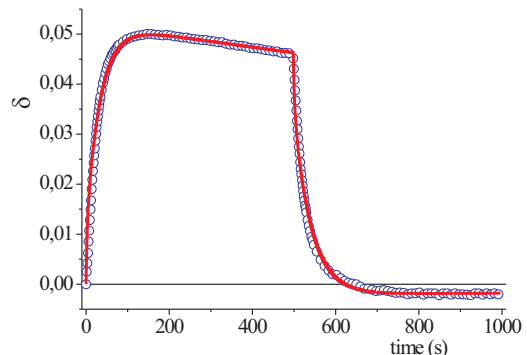


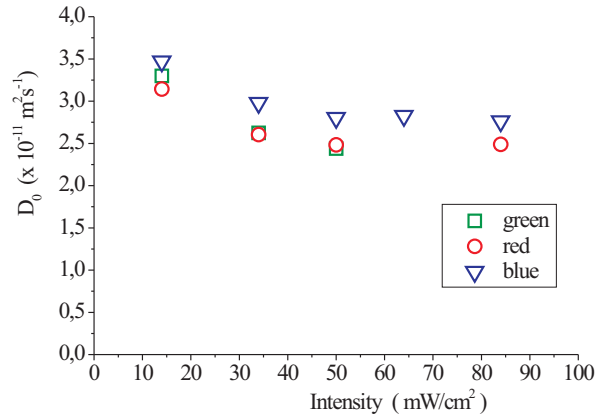
FIG. 7: (Color online) Example of the fitting of the calculated signal (solid line) to the experimental data (circles).

A comparison of the predictions of the theoretical model with the experimental observations is given in Fig. 9 for traces obtained with blue desorbing light. Except for the largest intensities, where the effects of saturation and illumination history are expected to be significant, the model correctly describes the growth of the LIAD signal with light intensity. Similar results are obtained for the other colors used for illumination.

Our theoretical model appears to correctly account for several features of the experimental signal. As shown in Fig. 10 the signal shape variation as a function of the illumination time interval is well described. In particular, the “undershoot” ε of the vapor density below the initial density is well reproduced. Such “undershoot” is due to the small variation of the total number of atoms (due to the external pumping system) during illumination. As the illumination is turned off, the atoms are rapidly re-adsorbed by the porous alumina in a time shorter than

TABLE I: Fitted values of the parameters of the model.

$D_0[m^2 \cdot s^{-1}]$	$L_0[m]$	$\gamma[s^{-1}]$	$\sigma[mW^{-1}]$	$\kappa_{red}[mW^{-1}]$	$\kappa_{green}[mW^{-1}]$	$\kappa_{blue}[mW^{-1}]$
$2.8 \pm 0.5 \times 10^{-11}$	106 ± 33	$2.4 \pm 1.5 \times 10^{-4}$	$2.2 \pm 2.0 \times 10^{-3}$	$7.8 \pm 0.7 \times 10^{-3}$	$4.6 \pm 0.5 \times 10^{-3}$	$5.2 \pm 0.5 \times 10^{-3}$

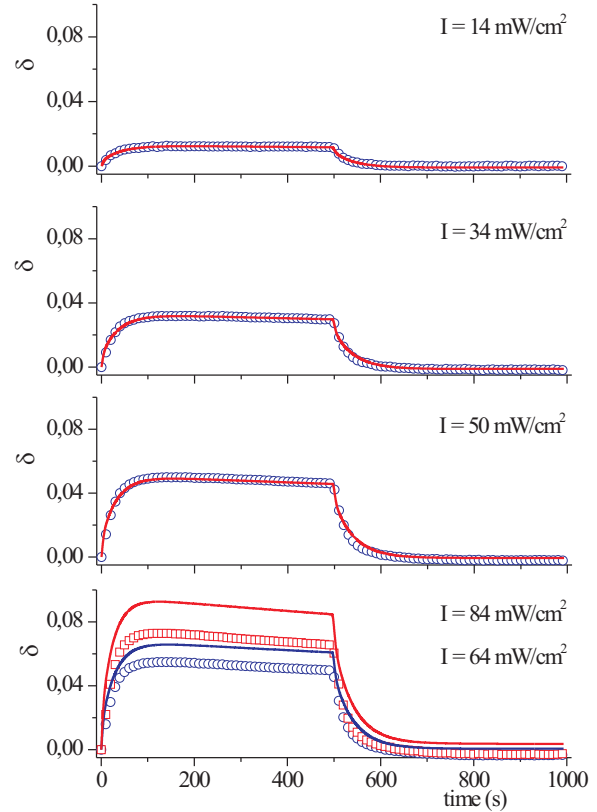
FIG. 8: (Color online) Values of the diffusion constant D_0 obtained from the fitting of different experimental traces obtained with three illumination colors.

the one required to equilibrate the cell with the external pump and Rb supply. The model also reproduces the difference in shape of the temporal evolution between low and large illumination intensities as shown in Fig 11. Such shape variations were previously observed but not reproduced by existing models [19].

From the measured value of D_0 using Eq. 1 one can determine the sticking time τ_s of the atoms to the pore walls. The obtained value $\tau_{s0} \simeq 500\mu s$ lies within the range of previous observations for alkali atoms on dielectric surfaces. A summary of the sticking times reported in the literature for several alkali atoms and surfaces is presented in Table II. The value of τ_s is several orders of magnitude larger than the mean time-of-flight of the atoms between collisions with the pore walls $\tau_0 \sim 1ns$. At a given time, the fraction of atoms in the gas phase inside the pores relative to the total number of atoms participating in the diffusion is $\tau_0/\tau_s \sim 10^{-5}$. From the values in Table I we estimate a relative variation of the atomic gas density within the pores of 60% for illumination with $50 mW/cm^2$ of red light.

V. CONCLUSIONS

We have studied LIAD of Rb atoms contained within alumina nanopores. We observed, as a function of time, the variations of the Rb density in the cell surrounding the porous alumina as illuminating light with different colors is turned on and off. We have shown that the

FIG. 9: (Color online) Comparison of the experimental data (circles and squares) with the calculated signal (solid lines) obtained with the parameters in Table I for $\lambda = 455nm$

observed signal evolution is determined by the diffusive motion of Rb atoms within the porous medium. Our observations are consistent with the picture of atoms undergoing a one dimensional random walk along the porous axis. Taking advantage of the well characterized geometry of the porous medium, a simple relation of the diffusion coefficient with the pore diameter and the atom-wall sticking time was established. Also, at the pores ends, the atom exchange between the gas cell and the porous medium is directly linked, without additional assumptions, to the parameters of the diffusive motion (Eq. 8).

The measurement of the diffusion constant gives direct access to the mean time between steps. This time is essentially a sticking time as the atoms remain most of the time absorbed to the pore wall. Our results indi-

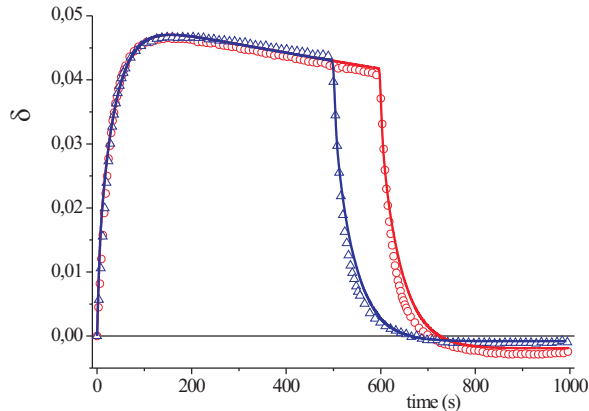


FIG. 10: (Color online) Observed (circles and triangles) and calculated (solid line) signals for two illumination intervals.

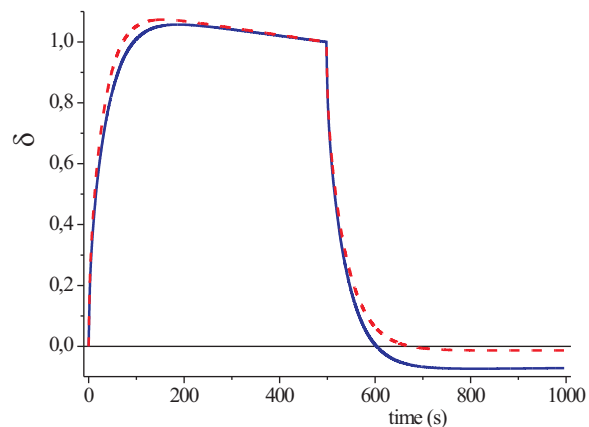


FIG. 11: (Color online) Calculated traces for different illumination intensities. The plots have been re-scaled to signal the difference in shape.

cate a linear decrease of the sticking time with the illuminating light intensity for low light intensity. In addition the sticking time modification appears to be dependent of the illuminating light frequency. The LIAD yield does not vary monotonically with light frequency for the three wavelength used. This suggests that the atom release takes place, at least in part, from rubidium clusters where surface plasmon resonances contribute to the light absorption spectrum [24, 25].

VI. ACKNOWLEDGEMENTS

The authors acknowledge support from ANII (Fondo Clemente Estable), CSIC and ECOS-Sud.

TABLE II: Reported alkali - dielectric surface sticking times at room temperature

Atom-Surface	Sticking time	Comments
Cs-Pyrex	1400 μ s	[28]
Cs-sapphire	< 160 μ s	[28]
Na-glass	130 μ s	[29]
Rb-alumina	500 μ s	This work

APPENDIX A: CALCULATION OF THE DIFFUSION COEFFICIENT IN A CYLINDRICAL PORE

For a one dimension random walk in the direction y , assuming that the length and duration of the random steps are uncorrelated, the diffusion constant is given by [30]:

$$D = \frac{\langle l_y^2 \rangle}{2\tau} = \frac{\langle v_y^2 t^2 \rangle}{2\tau} \quad (\text{A1})$$

where l_y is the single step displacement in the direction y , v_y is the y component of the particle velocity and t the time-of-flight of a given step. τ is the mean time interval between steps.

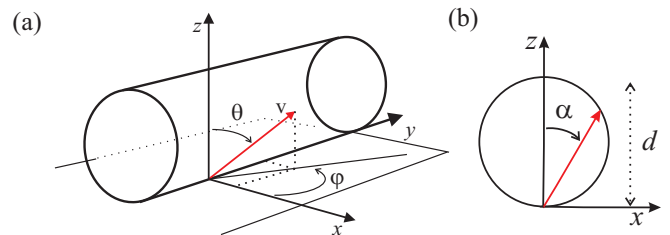


FIG. 12: (Color online) a) Cylinder and coordinate system considered in the calculation. b) Cross-section along the x, z plane.

We consider particles free flying within the inner surface of cylinder with diameter d . A particle leaving the cylinder wall has a velocity given by:

$$\begin{aligned} v_z &= v \cos(\theta) \\ v_y &= v \sin(\theta) \sin(\phi) \\ v_x &= v \sin(\theta) \cos(\phi) \end{aligned} \quad (\text{A2})$$

where v is the velocity modulus. See Fig. 12 for angle definitions.

The time-of-flight is given by:

$$t = \frac{l_{x,z}}{v_{x,z}} \quad (\text{A3})$$

where $l_{x,z}$ and $v_{x,z}$ are the projections of the particle displacement and velocity over the x, z plane. We have:

$$l_{x,z} = d \cos(\alpha) = d \frac{v_z}{v_{x,z}} \quad (\text{A4})$$

Using Eqs. A2, A3 and A4 we obtain:

$$t = \frac{d \cos(\theta)}{v (\cos^2(\theta) + \sin^2(\theta) \cos^2(\phi))} \quad (\text{A5})$$

and

$$l_y = v_y t = \frac{d \sin(\theta) \cos(\theta) \sin(\phi)}{(\cos^2(\theta) + \sin^2(\theta) \cos^2(\phi))} \quad (\text{A6})$$

The angular (Lambertian) distribution of the atoms leaving the surface is given by [27]:

$$P(\Omega) d\Omega = \cos(\theta) d\Omega \quad (\text{A7})$$

where Ω is the solid angle. The thermal distribution for the magnitude of the atomic velocity is [27]:

$$P(v) = \frac{1}{2} \left(\frac{m}{k_B T} \right)^2 v^3 \exp \left(-\frac{v^2}{v_{rms}^2} \right) \quad (\text{A8})$$

with $v_{rms} = \sqrt{\frac{2k_B T}{m}}$.

Using A6 and A7, after integration one gets:

$$\langle l_y^2 \rangle = \frac{2}{3} d^2 \quad (\text{A9})$$

In a similar way, from A5, A7 and A8 we obtain:

$$\tau_0 = \langle t \rangle = d \sqrt{\frac{2\pi m}{k_B T}} \quad (\text{A10})$$

In our system, the time interval between flights is determined by the atom sticking time τ_s ($\tau \simeq \tau_s \gg \tau_0$).

-
- [1] A. Gozzini, F. Mango, J. H. Xu, G. Alzetta, F. Maccarone, and R. A. Bernheim, *Nuovo Cimento* **15**, 709 (1993).
- [2] B. P. Anderson and M. A. Kasevich, *Phys. Rev. A* **63**, 023404 (2001).
- [3] S. N. Atutov, R. Calabrese, V. Guidi, B. Mai, A. G. Rudavets, E. Scansani, L. Tomassetti, V. Biancalana, A. Burchianti, C. Marinelli, et al., *Phys. Rev. A* **67**, 053401 (2003).
- [4] C. Klempt, T. van Zoest, T. Henninger, O. Topic, E. Rasel, W. Ertmer, and J. Arlt, *Phys. Rev. A* **73**, 013410 (2006).
- [5] S. Ghosh, A. R. Bhagwat, C. K. Renshaw, S. Goh, A. L. Gaeta, and B. J. Kirby, *Phys. Rev. Lett.* **97**, 023603 (2006).
- [6] P. Londero, V. Venkataraman, A. R. Bhagwat, A. D. Slepko, and A. L. Gaeta, *Physical Review Letters* **103**, 043602 (pages 4) (2009), URL <http://link.aps.org/abstract/PRL/v103/e043602>.
- [7] A. R. Bhagwat, A. D. Slepko, V. Venkataraman, P. Londero, and A. L. Gaeta, *Physical Review A (Atomic, Molecular, and Optical Physics)* **79**, 063809 (pages 6) (2009), URL <http://link.aps.org/abstract/PRA/v79/e063809>.
- [8] T. Karaulanov, M. T. Graf, D. English, S. M. Rochester, Y. J. Rosen, K. Tsigtukin, D. Budker, E. B. Alexandrov, M. V. Balabas, D. F. J. Kimball, et al., *Physical Review A (Atomic, Molecular, and Optical Physics)* **79**, 012902 (pages 9) (2009), URL <http://link.aps.org/abstract/PRA/v79/e012902>.
- [9] A. Bogi, C. Marinelli, A. Burchianti, E. Mariotti, L. Moi, S. Gozzini, L. Marmugi, and A. Lucchesini, *Opt. Lett.* **34**, 2643 (2009), URL <http://ol.osa.org/abstract.cfm?URI=ol-34-17-2643>.
- [10] B. V. Yakishinskiy and T. E. Madey, *Surf. Sci.* **528**, 54 (2003).
- [11] J. H. Xu, A. Gozzini, F. Mango, G. Alzetta, and R. A. Bernheim, *Phys. Rev. A* **54**, 3146 (1996).
- [12] E. B. Alexandrov, M. V. Balabas, D. Budker, D. English, D. F. Kimball, C.-H. Li, and V. V. Yashchuk, *Phys. Rev. A* **66**, 042903 (2002).
- [13] A. M. Bonch-Bruевич, T. A. Vartanyan, Y. N. Maksimov, S. G. Przhibelskii, and V. V. Khormov, *Sov. Phys. JEPT* **70**, 993 (1990).
- [14] S. N. Atutov, V. Biancalana, P. Bicchi, C. Marinelli, E. Mariotti, M. Meucci, A. Nagel, K. A. Nasyrov, S. Rachini, and L. Moi, *Phys. Rev. A* **60**, 4693 (1999).
- [15] E. Mariotti, M. Meucci, C. Marinelli, P. Bicci, and L. Moi, in *Proceedings of the XII International Conference on Laser Spectroscopy* (World Scientific New York, 1996), p. 390.
- [16] S. Gozzini and A. Lucchesini, *Eur. Phys. J. D.* **28**, 157 (2004).
- [17] J. H. Xu, Ph.D. thesis, Scuola Normale Superiore (1994).
- [18] A. M. Bonch-Bruевич, Y. N. Maksimov, S. G. Przhibelskii, and V. V. Khormov, *Sov. Phys. JEPT* **65**, 161 (1987).
- [19] A. Burchianti, C. Marinelli, A. Bogi, J. Brewer, K. Rubahn, H. G. Rubahn, F. D. Valle, E. Mariotti, V. Biancalana, S. Veronesi, et al., *Europhys. Lett.* **67**, 983 (2004).
- [20] R. J. Hamers, *Surf. Science* p. 583 (2005).
- [21] J. Brewer, V. G. Bordo, M. J. Kasproicz, and H. G. Rubahn, *Phys. Rev. A* **69**, 062902 (2004).
- [22] K. Rebilas and M. J. Kasproicz, *Physical Review A (Atomic, Molecular, and Optical Physics)* **79**, 042903 (pages 8) (2009), URL <http://link.aps.org/abstract/PRA/v79/e042903>.
- [23] K. Rebilas, *Phys. Rev. A* **80**, 014901 (2009).
- [24] A. Burchianti, A. Bogi, C. Marinelli, E. Mariotti, and

- L. Moi, *Optics Express* **16**, 1377 (2008).
- [25] A. Burchianti, A. Bogi, C. Marinelli, C. Maibohm, E. Mariotti, and L. Moi, *Physical Review Letters* **97**, 157404 (pages 4) (2006), URL <http://link.aps.org/abstract/PRL/v97/e157404>.
- [26] A. Burchianti, A. Bogi, C. Marinelli, C. Maibohm, E. Mariotti, S. Sanguinetti, and L. Moi, *European Physical Journal D* **49**, 201 (2009).
- [27] F. O. Goodman and H. Y. Wachman, *Dynamics of Gas-Surface Scattering* (Academic Press, 1976).
- [28] M. Stephens, R. Rhodes, and C. Wieman, *Journal of Applied Physics* **76**, 3479 (1994).
- [29] V. G. Bordo and H. G. Rubhan, *Optics Express* **4 No2**, 59 (1999).
- [30] E. Ott, *Chaos in dynamical systems* (Cambridge University Press, Cambridge, 1993), ISBN 0-521-43215-4.